

# Initial Results from the Chandra High Energy Transmission Grating Spectrometer

C.R. Canizares, D.S. Davis, D. Dewey, K.A. Flanagan, J. Houck, D.P. Huenemoerder,  
H.L. Marshall, M.L. Schattenburg, N.S. Schulz, M. Wise

*MIT Center for Space Research*

**Abstract.** The High Energy Transmission Grating Spectrometer (HETGS) on the Chandra X-ray Observatory provides spectral resolving powers of 200-1000 over the range 0.4-8.0 keV (1.5-30 Å) with effective area of 2-200 cm<sup>2</sup>. Initial observations during the activation and calibration phases of the mission show that the HETGS is performing as predicted prior to Chandra launch. The talk presented very preliminary results that illustrate the power of the HETGS for performing detailed studies of a wide range of celestial sources, including plasma diagnostics. This written version gives a brief summary of that talk with examples of preliminary spectra of Capella, the Crab pulsar, SS433 and the SNR E0102-72.

## 1. The Chandra HETGS

The High Energy Transmission Grating (HETG) on the Chandra X-ray Observatory consists of an array of periodic gold microstructures that can be interposed in the converging X-ray beam just behind the High Resolution Mirror Assembly (see Canizares et al. 2000a). When in place, the HETG disperses the X-rays according to their wavelength, creating a spectrum that is recorded at the focal plane by the linear array of CCDs designated ACIS-S (HETGS refers to the full system). There are two different grating types optimized for medium and high energies, designated MEG and HEG. These have periods of 4000 Å and 2000 Å respectively. The grating elements are gold, and are of appropriate thickness to “blaze” the grating in its energy range, enhancing the diffraction efficiency in the first orders (this results from destructive interference in zeroth order between the radiation that passes through the gaps and the grating bars). The MEG covers the outer two Chandra mirror segments, which provide most of the effective area at mid and lower energies, and the HEG the inner two, which give all the high energy area. The gratings were fabricated in the MIT Center for Space Research Space Nanostructures Laboratory using an extension of techniques used for VLSI circuit fabrication.

The HETGS provides spectral resolving power of 200-1000 for point sources (about 0.02 Å for MEG, and 0.01 Å for HEG) and effective areas of 2-200 cm<sup>2</sup> over the band 0.4-8 keV. The HETG positive and negative orders of the dispersed spectrum appear in the focal plane on either side of the undispersed zeroth order source image. The grating patterns of the HEG and MEG are offset in angle from each other by 10 deg. so their spectra make a shallow “X”-pattern at the focal plane. Multiple overlapping orders are removed by using the moderate energy resolution of the ACIS detector. The HETGS complements the LETGS, which is optimized for lower energy X-rays. For a full description of Chandra see the “Proposer’s Observatory Guide” and references therein (available at <http://chandra.harvard.edu>).

Preliminary analysis of in-flight calibration data indicate that the HETGS is performing as predicted prior to the Chandra launch, with effective areas within ~ 10% of the expected values except from 6-12 Å where there are systematic uncertainties of up to 20% still to be reduced by calibration. We note that the increased charge transfer inefficiency in the ACIS CCDs caused by unforeseen radiation damage early in the mission has no significant impact on the performance of the HETGS.

The data presented here were processed and analyzed with a combination of standard CXC and custom software. Each detected photon is assigned a dispersion angle,  $\theta$ , relative to the undiffracted zero-order image. The angle is related to the order,  $m$ , and wavelength,  $\lambda$ , through the grating mean period,  $P$ , by the simple grating equation,  $m\lambda = P \sin \theta$ . The order is determined using the approximate

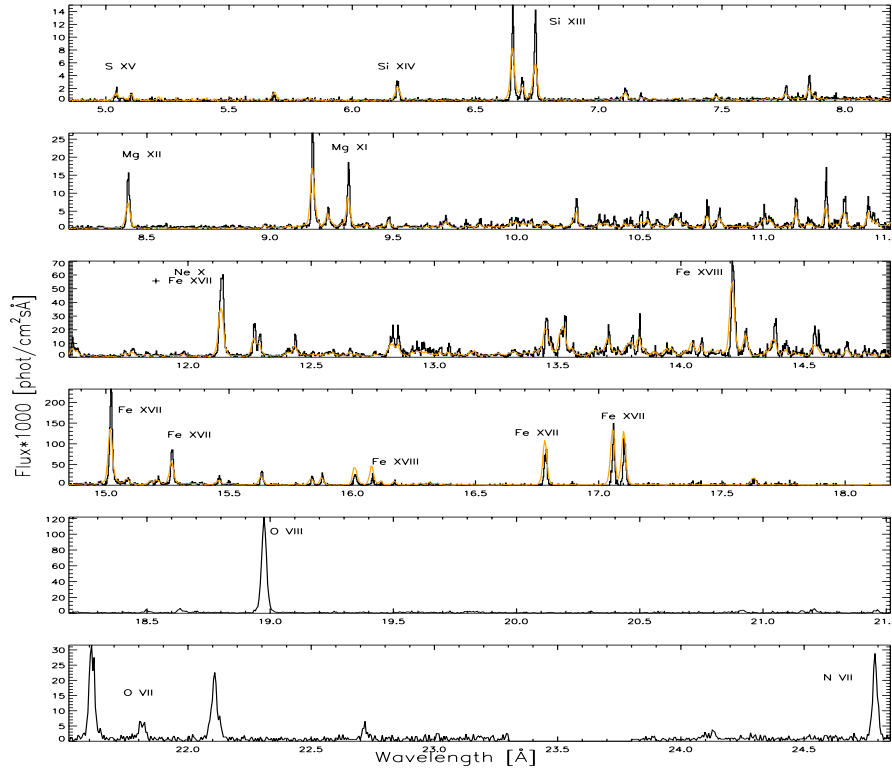


Figure 1. The HEG (dark line) and MEG (light line) spectrum of Capella (top four panels) and MEG only (bottom two panels). Data for  $\pm 1^{st}$  orders are summed for a total of 89 ks

energy measured by the ACIS-S CCD's. The counts are divided by the effective area to provide a photon flux per bin. Some small remaining calibration errors in wavelength and effective area have not yet been removed.

## 2. Capella

Capella ( $\alpha$  Aurigae) is an RS CVn binary system with an active corona well studied in the ultraviolet and with previous X-ray telescopes (see Brickhouse et al. 2000, and references therein). A first analysis of the HETGS observation of Capella is presented in Canizares et al. (2000b). Complementary results from the LETGS are in Brinkman et al. (2000).

We combined data from three HETGS observations totaling 89 ksec. The dispersed spectrum is shown in Figure 1.

The spectrum shows a forest of lines and line blends, including the strong transitions from H-like and He-like ions of N, O, Mg, Ne, Si, S, and the L lines of several ionization states of Fe, from Fe XVII through Fe XIX. The HEG and MEG complement each other in resolution and in area. The HEG can be used to resolve lines blended in the MEG, while the MEG generally has more effective area in the central portion of the Chandra band (for example, scrutinize the 6.7Å and 12.3Å region in Figure 1).

Even a cursory examination of the spectrum gives some new information about Capella's corona. The spectrum contains lines with a wide range of ionization levels, from N VII  $\lambda$ 24.8 through Ne X  $\lambda$ 13.4 to S XV  $\lambda$ 5.0. The temperatures of maximum emissivity for these three lines are  $\log T=6.3$ , 6.8 and 7.2, respectively, suggesting emission from plasma with a significant range of temperature. It is clear that plasma must be present over nearly a decade in temperature. This is consistent with ultraviolet spectra

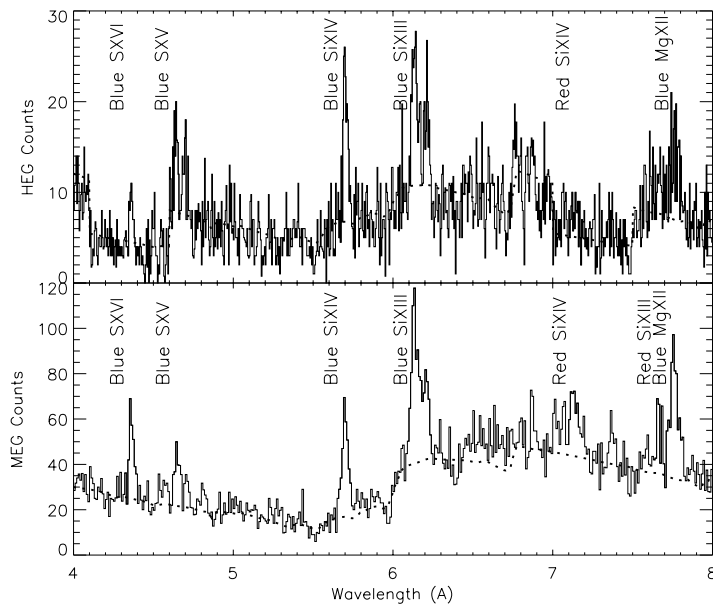


Figure 2. A portion of the HEG (top) and MEG (bottom) spectra of SS 433 observed with the Chandra HETGS, showing the blue-shifted H- and He-like lines of S (S XVI and S XV), the corresponding lines of Si (Si XIV and Si XIII) as well as the red-shifted counterparts to the Si lines. Note that the lines are broadened and that the He-like triplets of S and Si are resolved.

from EUVE (Brickhouse et al. 2000). But prior to Chandra the X-ray data were equally well explained with only two temperature components (Swank et al. 1981; Schmitt et al. 1990).

An approximate upper envelope to the true VEM distribution is given by the family of curves formed by plotting the ratio of line strength to corresponding emissivity for a collection of lines (see for example, Griffiths and Jordan 1998; Vedder and Canizares 1983). For a given element, the abundance affects only the overall normalization of the envelope of all lines from that element. We find reasonable agreement with the emission measure distribution deduced from EUVE emission lines by Brickhouse et al. (2000). The Fe xxv  $\lambda 1.85$  line is not detected, which sets an upper limit on any high temperature emission during this observation.

Clearly, a much more detailed analysis is required, leading to a good determination of the emission measure distribution. The He-like lines discussed by Pradhan and others at this meeting are well resolved for nearly all the alpha-group elements, and can be used as temperature and density diagnostics (Pradhan 1982; Doschek 1990). And we can look for or set limits on the optical depth to resonant scattering, which constrains the column density (Saba et al. 1999). These diagnostics will help us understand the structure of Capella's corona, such as the characteristic dimensions of the coronal loops.

### 3. SS433

SS433 is another interesting target for the HETGS. This is a Galactic binary with a compact object (either neutron star or black hole) and relativistic jets (Margon 1984). Strong red and blue shifted lines are well studied in the optical and have been seen at moderate spectral resolution by ASCA (Kotani 1996). The lines move back and forth with a 163d period, the result of precession of the emitting jet.

The HETG MEG spectrum is shown in Figure 2. There are prominent red and blue shifted lines from Mg, Si and S, corresponding to  $v/c = 0.26$ , which is the expected value for the jet precession phase at the time of the observation. The observed red and blue shifts are offset due to the transverse Doppler effect, and the relative enhancement of the blue shifted compared to the redshifted lines is expected

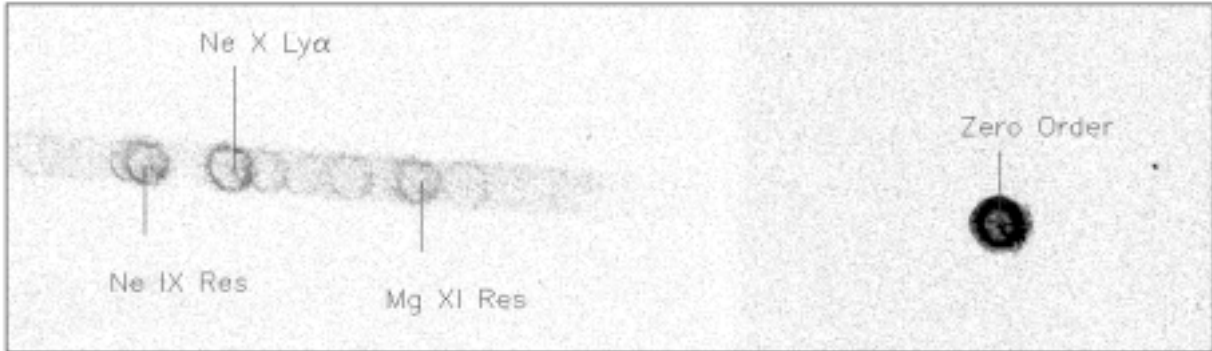


Figure 3. A portion of the MEG spectrum of E0102-72

from Doppler boosting. The lines are clearly resolved, with line widths corresponding to  $\sim 1000 \text{ km s}^{-1}$ , which is similar to the values seen in the optical spectrum, but was previously unresolved in X-rays.

We are planning to obtain additional observations at other precession phases during the next observing period. The hope will be to use spectra such as this one to deduce the structure of the jets and maybe learn something about the acceleration processes.

#### 4. The Crab Pulsar

Not all spectra we have obtained so far contain the rich emission lines seen in stellar coronae like Capella or in SS433. For example, the spectrum extracted for the Crab pulsar is comparatively featureless. To within the current uncertainties of the calibration, it appears to be a perfect power law absorbed by interstellar material. There is evidence for structure in the interstellar absorption, as expected and as was first observed with much less sensitivity and spectral resolution by the FPCS on *Einstein* (Schattenburg 1986) around the oxygen absorption edge. Observations like these should be good probes of the abundance and possibly even the physical state (gaseous vs. bound in grains) of the absorbing material.

#### 5. The Supernova Remnant E0102-72

Although the HETGS (and LETGS) work best on point sources, it is also extremely useful for studying moderately extended sources, particularly objects like supernova remnants (SNRs), which like the stellar corona are optically thin plasmas dominated by strong emission lines.

An early target is E0102-72 in the Small Magellanic Cloud, which is one of a handful of oxygen rich remnants thought to be the product of a type II SN in a massive star (Dopita 1981; Hyashi 1994). A portion of the dispersed spectrum is shown in Figure 3. One sees an image of the remnant in zeroth order, and then multiple images reproduced in the “light” of individual strong X-ray lines, in analogy to a spectroheliogram of the sun.

Several things have emerged from our very preliminary analysis. First, we see very strong O, Ne, and Mg, but little or no Fe. There are slight differences in the images for different ions of the same element, much less for different elements. This shows that ionization conditions vary over the remnant, as had been suspected from inconsistencies in the non-equilibrium models deduced for different species with ASCA (Hyashi 1994). A preliminary analysis also shows Doppler shifts of individual bright clumps in the ejecta on either side of the ring, indicating a complex velocity structure with amplitudes of  $1000 - 2000 \text{ km s}^{-1}$ .

**Acknowledgments.** This work was supported by NASA through contract NAS8-38249 and through the Chandra X-ray Center contract SV1-61010 from the Smithsonian Astrophysical Observatory. We thank the entire Chandra team, especially all our colleagues who helped develop the HETG.

**References**

- Brickhouse, N.S., Dupree, A.K., Edgar, R.J., Liedahl, D.A. Drake, S.A., White, N.E., Singh, K.P. 2000, *ApJ* , 387.
- Brinkman, A.C., et al. 2000, *ApJ* (submitted)
- Canizares, C.R. et al. 2000a, in preparation
- Canizares, C.R. et al. 2000b, *ApJ* (submitted)
- Dopita, M.A., Tuohy, I.R., Mathewson, D.S. 1981 *ApJ* 248, L105
- Doschek, G.A. 1990, *ApJS* , 73, 117
- Griffiths, N.W., Jordan, C. 1998 *ApJ* , 497, 883
- Hyashi, I. et al. 1994, *PASJ*, 46, L121
- Kotani, T., Kawai, N., Matsuoka, M., Brinkman, W. 1996, *PASJ*, 48, 619
- Margon, B. 1984, *ARA&A* 22, 507
- Pradhan, A. K. 1982, *ApJ* , 263, 497
- Saba, J.L.R., Schmelz, J.T., Bhatia, A.K., and Strong, K.T., 1999 *ApJ* , 510, 1064.
- Schmitt, et al. 1990, *ApJ* , 365, 704
- Schattenburg, M.L., Canizares, C.R. 1986, *ApJ* 301, 759
- Swank et al., 1981, *ApJ* , 246, 214
- Vedder, P.W., Canizares, C.R. 1983, *ApJ* , 270, 666